



**HAL**  
open science

## Ozone-assisted oxidation of ethylene in a jet-stirred reactor: An experimental and modeling study

Caroline Smith Lewin, Olivier Herbinet, Frédérique Battin-Leclerc, Jérémy Bourgalais

► **To cite this version:**

Caroline Smith Lewin, Olivier Herbinet, Frédérique Battin-Leclerc, Jérémy Bourgalais. Ozone-assisted oxidation of ethylene in a jet-stirred reactor: An experimental and modeling study. *Chemical Physics Letters*, 2022, 806 (18), pp.139986. 10.1016/j.cplett.2022.139986 . hal-03847088

**HAL Id: hal-03847088**

**<https://hal.science/hal-03847088>**

Submitted on 10 Nov 2022

**HAL** is a multi-disciplinary open access archive for the deposit and dissemination of scientific research documents, whether they are published or not. The documents may come from teaching and research institutions in France or abroad, or from public or private research centers.

L'archive ouverte pluridisciplinaire **HAL**, est destinée au dépôt et à la diffusion de documents scientifiques de niveau recherche, publiés ou non, émanant des établissements d'enseignement et de recherche français ou étrangers, des laboratoires publics ou privés.



Distributed under a Creative Commons Attribution - NonCommercial - NoDerivatives 4.0 International License

1 Ozone-Assisted Oxidation of Ethylene in a Jet-Stirred  
2 Reactor: an Experimental and Modeling Study

3  
4 Caroline Smith Lewin, Olivier Herbinet, Frédérique Battin-Leclerc, and Jérémy Bourgalais\*

5  
6 Université de Lorraine, CNRS, LRGP, F-54000 Nancy, France.  
7  
8  
9  
10  
11  
12  
13  
14  
15  
16  
17  
18  
19  
20  
21  
22  
23  
24  
25  
26  
27  
28

---

29 \*Corresponding author: Jérémy Bourgalais

30 e-mail: [jeremy.bourgalais@cnr.fr](mailto:jeremy.bourgalais@cnr.fr)

31 [ORCID: 0000-0003-4710-8943](https://orcid.org/0000-0003-4710-8943)

32 [Phone: \(33\)3-72-74-38-17](tel:+33372743817)

33           **KEYWORDS**

34           Ozonolysis; Jet-stirred reactor; mass-spectrometry; gas chromatography; kinetic  
35 model

36           **ABSTRACT**

37           Ozone addition is a promising method to achieve improvement and control of  
38 combustion/ignition processes due to ozone-derived chemistry. However, the complexity  
39 induced by ozonolysis reactions make investigations on O<sub>3</sub>-assisted oxidation with alkenes still  
40 scarce. In this work, the ozone-assisted oxidation of ethylene was studied in a jet-stirred  
41 reactor from 300 to 1000 K. The main products were identified and quantified by mass  
42 spectrometry/gas chromatography analysis. The mole fractions were then compared to those  
43 computed with a kinetic model from the literature. This work provides data for the  
44 development of detailed chemical kinetic models relevant to atmospheric and combustion  
45 chemistry studies.

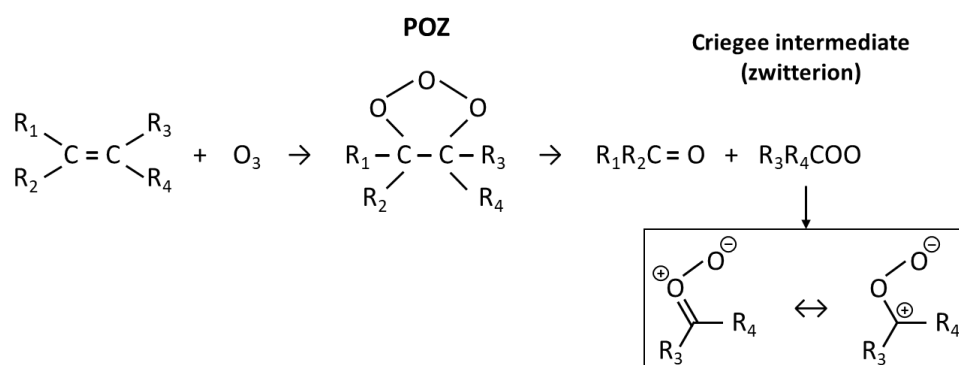
46  
47           **INTRODUCTION**

48           The so-called ozonolysis process during the gas-phase oxidation of organic compounds  
49 in presence of ozone (O<sub>3</sub>) has been the subject of numerous studies for over a century in  
50 different scientific fields. The exothermic 1,3-dipolar cycloaddition of O<sub>3</sub> reaction onto  
51 unsaturated volatile organic compounds leads to the formation of reactive species called  
52 Criegee intermediates through a three-step mechanism [1,2]. Criegee intermediates affect the  
53 oxidative capacity of the atmosphere by being both a direct source of oxygenated compounds  
54 and radicals and by reacting with other species to form low-volatility compounds leading to  
55 the growth of aerosols and particles that impact the radiation balance and air quality (e.g., [3–  
56 6]). O<sub>3</sub>-assisted oxidation of hydrocarbons is also a subject of recent interest in low-  
57 temperature combustion studies due to the recent rise of investigations into non-equilibrium  
58 plasma-assisted combustion techniques and chemically controlled engine designs for  
59 emission control and efficiency enhancement [7–11]. Efficiently generated by electric  
60 discharge, O<sub>3</sub> is a low-temperature reaction promoter and an enhancer of combustion  
61 processes through the formation of various reactive intermediates [12–14]. This enhancement  
62 is related to O<sub>3</sub> chemistry, with the production of oxygen atoms from the thermal  
63 decomposition of O<sub>3</sub> at elevated temperatures accelerating the overall chain-propagating  
64 process, as well as the rapid exothermic ozonolysis reactions initiating direct reactions

65 between fuel and O<sub>3</sub> at low temperatures (even at room temperature). While the direct  
 66 reaction between O<sub>3</sub> and saturated hydrocarbons is almost negligible, the nearly barrierless  
 67 reaction with unsaturated species (a difference of several orders of magnitude [15]) is very  
 68 fast. Although considerable studies have been conducted on O<sub>3</sub>-assisted oxidation of alkanes  
 69 [16–23], investigations on alkenes are scarce, partially due to the much higher chemical  
 70 complexity induced by these ozonolysis reactions.

71 Most ozonolysis reactions involve the formation of a primary cyclic 1,2,3-trioxy  
 72 ozonide (POZ) from the van der Waals O<sub>3</sub>-alkene complex resulting from the addition of O<sub>3</sub>  
 73 onto the C=C bond. POZ then decomposes to form a carbonyl compound (R<sub>1</sub>R<sub>2</sub>C=O) and  
 74 carbonyl oxide (R<sub>3</sub>R<sub>4</sub>COO), the famous Criegee intermediate (CI), via homolytic cleavage of C-  
 75 C and C-O bonds (see FIGURE 1). After that, the quenching processes of the Criegee  
 76 intermediate give access to many reaction pathways, such as the formation of 1,2,4-trioxy  
 77 cyclic secondary ozonide (SOZ) [24–31]. A single O-O bond of the POZ can also break to give a  
 78 POZ biradical, making the accessible kinetic networks even more complicated [32,33]. For  
 79 recent reviews of CI's reaction pathways, readers may refer to Osborn & Taatjes [34] and  
 80 Taatjes [35].

81



82

83 FIGURE 1. Formation of POZ and Criegee intermediate from ozonolysis reaction.

84

85 Due to the multiplicity of kinetic pathways involved in ozonolysis, grey areas remain  
 86 even in the chemistry of the simplest O<sub>3</sub>-alkene system. The chemical pathways following the  
 87 reaction of O<sub>3</sub> with ethylene (CH<sub>2</sub>=CH<sub>2</sub>), despite being extensively studied for decades (see  
 88 [36–41] for the most recent studies) are still not fully understood and significant  
 89 disagreements remain between quantitative experiments and kinetic model predictions. The  
 90 most recent quantitative investigation on the O<sub>3</sub>-assisted oxidation of C<sub>2</sub>H<sub>4</sub> was reported by

91 Rousso et al. [39]. The oxidation of  $C_2H_4$  was carried out in a near atmospheric pressure (933  
92 mbar) jet-stirred reactor (JSR) from 300 to 1000 K by adding 1000 ppm of  $O_3$ . The mole fraction  
93 as a function of temperature of the oxidation products were obtained by electron-ionization  
94 mass spectrometry analysis. Their data were compared to the predictions of a kinetic model  
95 developed at Princeton [42–44], in which ozonolysis reactions were described using global  
96 reactions based on IUPAC recommendations. They reported significant discrepancies between  
97 the experimental data and the predictions, even for the consumption of  $C_2H_4$  and  $O_3$ , from  
98 low to intermediate temperatures ( $< 700$  K) suggesting missing major reaction pathways in  
99 the kinetic model. However, no mechanistic insight has been provided and many questions  
100 remain regarding the formation pathways of intermediates in this system.

101 The aim of this work is to focus on the mostly unknown kinetic networks initiated by  
102 ozonolysis reactions over a wide temperature range. While O atoms from the  $O_3$  thermal  
103 decomposition are of interest in lowering the fuel conversion temperature, ozonolysis can  
104 initiate alkene-based fuel conversion at even lower temperatures and may have an impact on  
105 auto-ignition [45]. In this work, new experimental data are generated over a wider range of  
106 experimental conditions for the  $O_3$ -assisted oxidation of  $C_2H_4$  to confront the predictions of  
107 current kinetic models. Especially, due to a different experimental configuration, the newly  
108 obtained data shows that a global ozonolysis mechanism can accurately simulate the mole  
109 fractions of the main products as well as the consumption of  $C_2H_4$  and  $O_3$ . The  $O_3$ -assisted  
110 oxidation of  $C_2H_4$  was carried out in a JSR between 300 K and 1000 K with varying the mole  
111 fraction of  $O_3$  from 1000 to 2000 ppm. The identification and the quantification of the main  
112 products and stable intermediates were performed by gas chromatography with mass  
113 spectrometry, thermal conductivity and flame ionization detections, and the obtained mole  
114 fractions were recorded as a function of temperature. The experimental data were then  
115 confronted to the predictions of the abovementioned kinetic model from the literature [42–  
116 44] to provide mechanistic insights into the  $O_3$ -assisted oxidation of  $C_2H_4$ .

117

## 118 **EXPERIMENTAL SETUP**

119 The experimental setup used in this work has been extensively described in the past,  
120 see for instance Bourgalais et al. [46], and only the essential information and modifications  
121 for the current experiments are given here. Constant pressure, residence time, and  
122 equivalence ratio of 1.067 bar, 2.5 s, and 0.5, respectively, were maintained for all the

123 experiments, with a continuous flowing gas mixture with mole fraction of 0.02 ethylene, 0.12  
124 O<sub>2</sub>, and 0.86 He in the JSR using calibrated Bronkhorst mass flow controllers (relative  
125 uncertainty of 0.5%). He and O<sub>2</sub> are provided by Messer (both 99.999% pure) and C<sub>2</sub>H<sub>4</sub> by Air  
126 Liquide with a purity of 99.95%. A JSR temperature range from 300 to 1000 K was investigated  
127 and the flow rates were adjusted to maintain a constant nominal residence time. A preheating  
128 zone upstream of the JSR inlet ensured the temperature gradient inside the vessel to be  
129 limited. The annular quartz tube has an approximate cross section of 0.25 cm<sup>2</sup> and a length of  
130 12 cm. The tube, as well as the JSR, is heated using THERMOCOAX resistances. To provide  
131 progressive preheating, its length is divided into two heating stages (6 cm long each) that are  
132 set to two different temperatures. For experiments without O<sub>3</sub>, the preheaters were set to  
133 temperatures close to the desired temperature in the JSR. However, for O<sub>3</sub>-assisted oxidation  
134 experiments, this procedure was followed only below the JSR temperature of 425 K, which is  
135 the threshold for the onset of O<sub>3</sub> thermal decomposition (as will be discussed later). From this  
136 temperature, to prevent O<sub>3</sub> decomposition before entering the reactor, the first preheater  
137 was set to 353 K and the second to 393 K, regardless of the JSR temperature. The reactor  
138 temperature was measured with a K-type thermocouple positioned in a glass finger close to  
139 the JSR center with an uncertainty of around 1%.

140 The C<sub>2</sub>H<sub>4</sub> ozonolysis experiments were achieved adding an O<sub>3</sub> mole fraction of 1000  
141 and 2000 ppm using an ozone generator (BMT 802N). Gas feeds of C<sub>2</sub>H<sub>4</sub> and O<sub>3</sub> were mixed  
142 just before entering the preheated zone of the JSR (see FIGURE 2 for a scheme of the  
143 experimental setup). An ozone analyzer (BMT 965 ST) based on a dual-beam UV photometer  
144 at 254 nm was used at the exit of the JSR to measure the O<sub>3</sub> mole fraction. The uncertainty of  
145 15% for the measurement of the O<sub>3</sub> mole fraction was derived including accuracy and  
146 repeatability error.

147

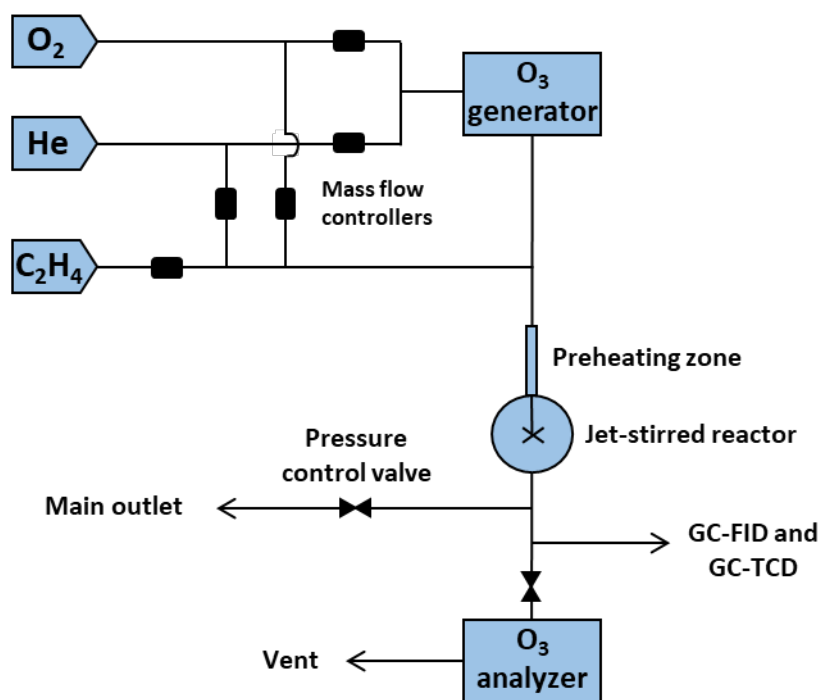


FIGURE 2. Scheme of the experimental setup.

148

149

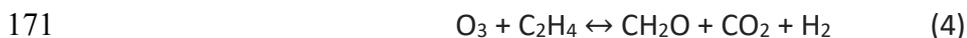
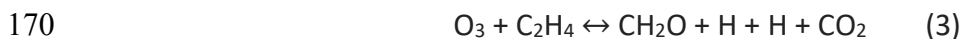
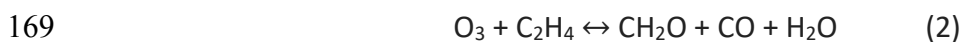
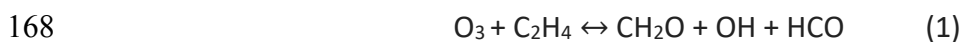
150

151  $C_2H_4$  and its oxidation products were quantified using two gas chromatographs (GCs)  
 152 connected to the exit of the JSR, one with a carbosphere-packed column and a thermal  
 153 conductivity detector (TCD) to quantify lightweight and permanent gas species, the second  
 154 with a Q-Bond capillary column and a flame ionization detector (FID) preceded by a  
 155 methanizer for the quantification of organic compounds. For species identification, a GC  
 156 equipped with a Q-Bond capillary column was coupled to a quadrupole mass spectrometer.  
 157 Ions were generated via electron impact ionization at 70 eV. The mole fractions of species  
 158 detected with the FID were calibrated using the effective carbon number (ECN) method. Their  
 159 calibration factors were deduced from that of  $C_2H_4$  by taking into account their effective  
 160 carbon number. The relative uncertainties in their mole fractions were estimated to be  $\pm 10\%$ .  
 161 The obtained carbon balance presented values from 87.8 to 107.0%, with an average of 99.6%

162

### 163 KINETIC MODEL

164 An up-to-date kinetic model developed at Princeton coupling an ethylene oxidation  
 165 mechanism and an  $O_3$  sub-mechanism was used to simulate the experimental data [42–44].  
 166 Based on IUPAC recommendation (<https://iupac.org/>), the following direct reactions between  
 167  $O_3$  and  $C_2H_4$  were implemented to simulate global ozonolysis reactions:



172 Using the CHEMKINPro software [47], the oxidation of  $\text{C}_2\text{H}_4$  without  $\text{O}_3$  was modelled  
173 considering a perfectly stirred reactor (see results in FIGURE S1 in Supplementary Material) as  
174 it is usually the case when modelling JSR, since the residence time in the preheating zone is  
175 only a few percent of that in the JSR [48]. In the  $\text{O}_3$ -assisted oxidation case, two plug flow  
176 reactors (PFR) were included ahead of the JSR to simulate the experimental preheating zone  
177 composed of two heating stages. This strategy of including a PFR was also used by Rousso et  
178 al. [39]. This was performed to account for the reactivity, especially the  $\text{O}_3$  thermal  
179 decomposition, before entering the JSR. The PFR simulations were based on the physical  
180 dimensions of the quartz tube from the entrance of the preheating zone to the JSR and utilizes  
181 the same temperature as used in the experiments. A numerical comparison between the  
182 composition at the outlet of the second PFR and that of the outlet of the JSR during  $\text{O}_3$ -assisted  
183 oxidation, as well as simulations using both reactor configurations (with and without PFRs),  
184 are presented in Supplementary Material. FIGURE S2 well demonstrates that a significant  
185 amount of  $\text{O}_3$  enters the JSR. As it can be seen in FIGURE S3, a slightly improved agreement  
186 when PFRs were considered is observed. Flow rates used in each experiment were also  
187 implemented in the model and were provided as inputs of the PFRs.

188

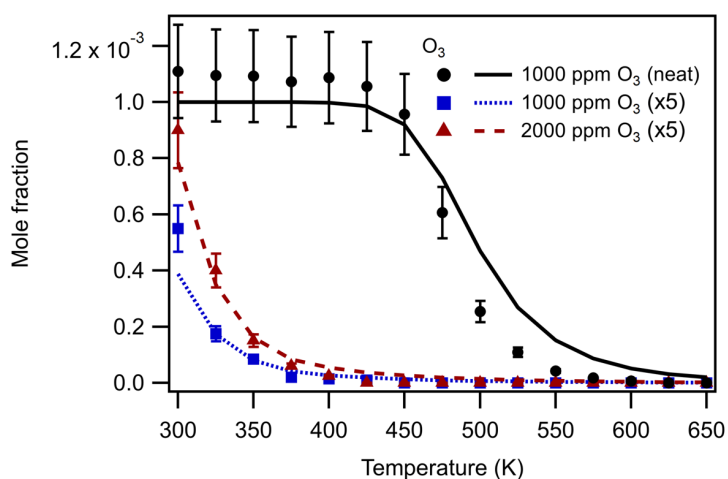
## 189 **RESULTS**

190 As a starting point, oxidation experiments without  $\text{O}_3$  addition were first conducted  
191 from 300 to 1000 K, as a reference for no low-temperature chemistry behavior. The evolution  
192 of the mole fractions of  $\text{C}_2\text{H}_4$ ,  $\text{O}_2$ , the intermediates ( $\text{CH}_2\text{O}$ ,  $\text{C}_3\text{H}_6$ ,  $\text{CH}_3\text{CHO}$ ,  $\text{CH}_4$ , and oxirane  
193  $\text{C}_2\text{H}_4\text{O}$ ), and the major products ( $\text{CO}$  and  $\text{CO}_2$ ) as a function of temperature are given in FIGURE  
194 S1. No decrease in the mole fraction of  $\text{C}_2\text{H}_4$  and  $\text{O}_2$  is observed below 800 K in the absence of  
195 ozone. Note that  $\text{H}_2\text{O}$  is also predicted as a major product with a mole fraction comparable of  
196 those of  $\text{CO}$  and  $\text{CO}_2$ , but it remains difficult to quantify it accurately by GC analysis. Oxirane  
197 was detected with a maximum mole fraction of 130 ppm at 850 K and mainly formed from  
198  $\text{HO}_2 + \text{C}_2\text{H}_4$  by direct epoxidation. An overall good agreement between experimental data and  
199 simulations is observed even if a slight overestimation of the predicted conversion of  $\text{C}_2\text{H}_4$  is

200 noticed between 800 and 850 K. At these temperatures, the conversion of  $C_2H_4$  is mainly  
201 driven by addition of OH on  $C_2H_4$ , as can be observed in the flow rate analysis of FIGURE S4,  
202 at 900 K. The rate constants provided in the literature for this reaction and currently  
203 implemented in the kinetic model correspond to the formation of all the three  $C_2H_5O$  isomers  
204 ( $CH_2CH_2OH$ ,  $OCH_2CH_3$ , and  $HOCHCH_3$ ) [49]. This might result in a slight overestimation of  
205  $CH_3CHO$  (see FIGURE S1). These results on the oxidation of neat  $C_2H_4$  give confidence to the  
206 experimental setup and the analysis procedure used in this work.

207 Thermal decomposition of  $O_3$  was also measured before considering the  $O_3$ -assisted  
208 oxidation of  $C_2H_4$ .  $O_3$  mole fraction as a function of temperature was recorded at the same  
209 residence time and pressure as in the ozonolysis case but without  $C_2H_4$ , using as gas mole  
210 fractions: 0.12  $O_2$ /0.001  $O_3$ /0.879 He. FIGURE 3 presents the  $O_3$  mole fraction as a function of  
211 temperature for neat  $O_3$  thermal decomposition and for  $C_2H_4$  oxidation with two  $O_3$  mole  
212 fractions (1000 and 2000 ppm). Consistent with previous data in the literature [39,44,50], the  
213 thermal decomposition of  $O_3$  starts  $\sim 450$  K and  $\sim 90\%$  of  $O_3$  is consumed by 550 K. This result  
214 indicates that above this temperature, fuel interactions with O-atoms can potentially compete  
215 with ozonolysis reactions in the formation of intermediate species and products.

216



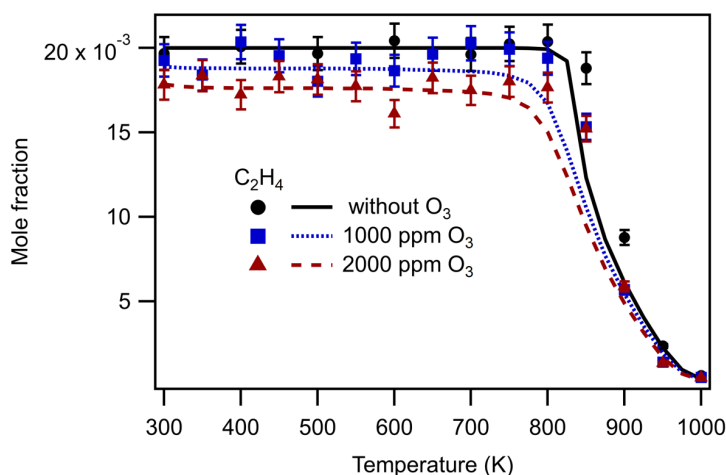
217  
218 FIGURE 3.  $O_3$  mole fraction as a function of temperature. Data in black correspond to the  
219 thermal decomposition of 1000 ppm of  $O_3$  (without  $C_2H_4$ ). Data in blue and red correspond  
220 to  $C_2H_4$  oxidation with 1000 ppm and 2000 ppm of  $O_3$ , respectively. The markers refer to the  
221 experimental data and the lines to simulations.

222

223 Compared to neat O<sub>3</sub> thermal decomposition, O<sub>3</sub>-assisted oxidation of C<sub>2</sub>H<sub>4</sub> in FIGURE  
224 3 shows that the addition of C<sub>2</sub>H<sub>4</sub> induces a drastic shift of the O<sub>3</sub> consumption toward lower  
225 temperatures, with a consumption of ~90% of O<sub>3</sub> at 300 K and ~99% at 350 K. The simulations  
226 show a relatively good agreement for O<sub>3</sub> consumption for both mole fraction conditions.  
227 Increasing by a factor of two the mole fraction of O<sub>3</sub> in presence of C<sub>2</sub>H<sub>4</sub> does not change the  
228 conversion yield of O<sub>3</sub>.

229 FIGURE 4 shows that with the addition of O<sub>3</sub>, the conversion of C<sub>2</sub>H<sub>4</sub> starts since room  
230 temperature. A decrease in the mole fraction of C<sub>2</sub>H<sub>4</sub>, 4.5% and 9% respectively, compared to  
231 the initial mole fraction is observed at 300 K. Multiplying the mole fraction of O<sub>3</sub> by two leads  
232 to a twofold decrease of C<sub>2</sub>H<sub>4</sub> at low temperatures. The C<sub>2</sub>H<sub>4</sub> conversion is stable between 400  
233 and 800 K, but decreases significantly from 850 K, indicating a transition to the high-  
234 temperature kinetic regime. No temperature shift is observed compared to the O<sub>3</sub>-free  
235 experiments, but the conversion is more important (a factor of 5 at 850 K) when O<sub>3</sub> is added.  
236 This difference reduces as the temperature increases, until it becomes almost negligible at  
237 about 950 K. A similar onset of the high-temperature reactivity under different O<sub>3</sub>-addition  
238 levels suggests that the addition of O-atom from the thermal decomposition of O<sub>3</sub> hardly  
239 alters the kinetics of the C<sub>2</sub>H<sub>4</sub> oxidation above 800 K.

240



241  
242 FIGURE 4. Consumption as a function of temperature of C<sub>2</sub>H<sub>4</sub> diluted in a gas mixture made  
243 of O<sub>2</sub>, O<sub>3</sub>, and He. Two inlet mole fractions of O<sub>3</sub> have been used: 1000 (blue squares) and  
244 2000 ppm (red triangles).

245

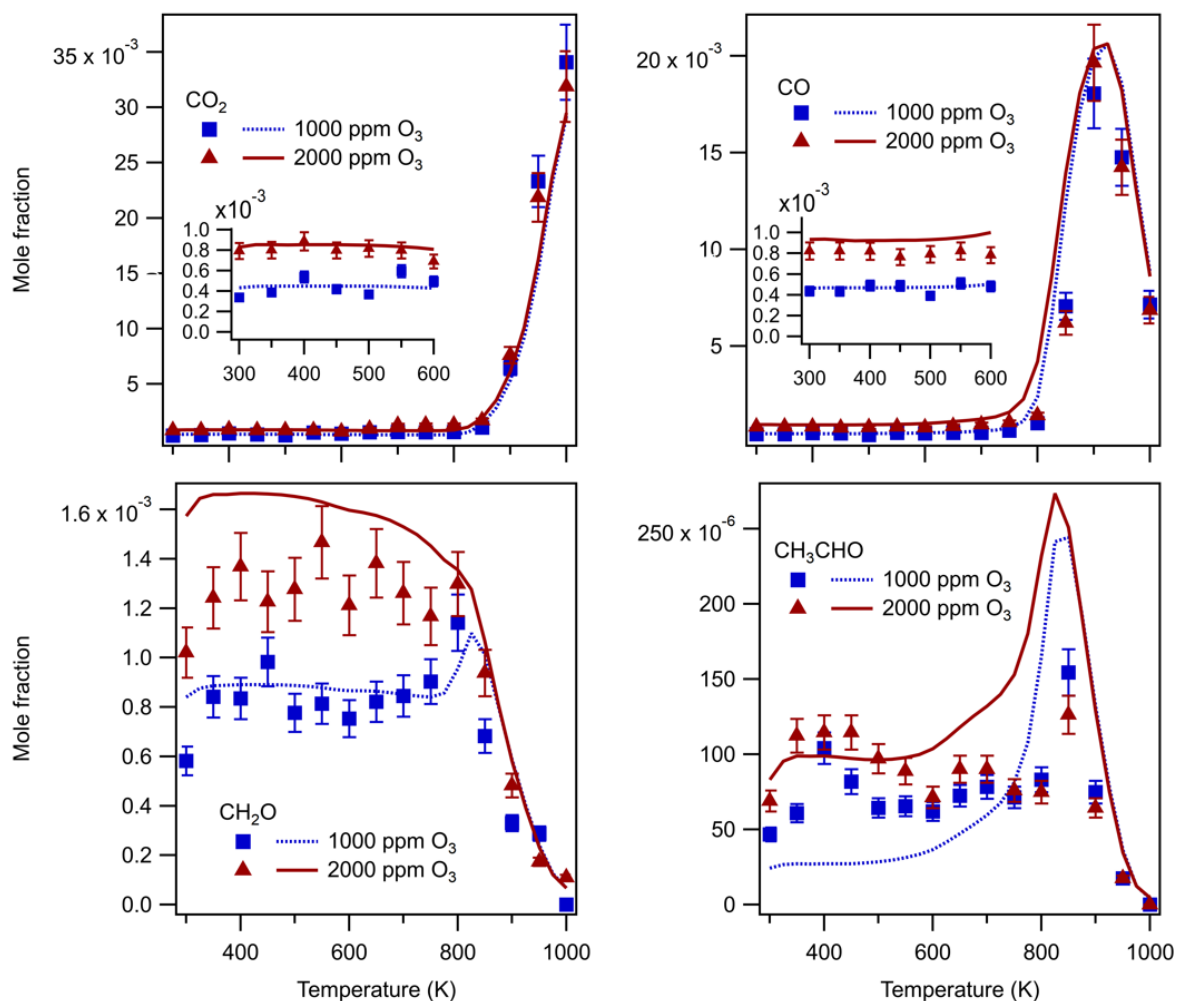


269 The good agreement observed in this work between simulation and experiments for  
270 the conversion of  $C_2H_4$  deviates from the work of Rouso et al. [39], who showed a poor  
271 agreement between experiments and simulation. Rouso et al. observed experimentally a  
272 decrease of the  $C_2H_4$  conversion as the temperature increased around 500 K. This increase of  
273 the  $C_2H_4$  mole fraction, however, does not seem to have any chemical explanation and might  
274 be due to the thermal decomposition of  $O_3$  in the injection line, as in their experimental setup  
275  $O_3$  and  $C_2H_4$  are injected through two separate heated lines into the JSR. The effect of the  
276 thermal decomposition of  $O_3$  is also reflected in Rouso et al. [39]'s profile of formaldehyde,  
277 which is the major product at low temperatures, and whose mole fraction drops to 0 between  
278 500 – 800 K in their study. Based on the global reactions implemented in the model to describe  
279 the ozonolysis process, a 1:1 mole fraction of  $CH_2O:C_2H_4(\text{consumed})$  is expected, but was not  
280 observed from 500 K by Rouso et al. [39]. In the present work, all gas lines were mixed before  
281 entering the preheating zone upstream of the reactor, in contrast to the separate injection of  
282  $O_3$  and  $C_2H_4$  in Rouso et al. [39]'s work. As shown in FIGURE 6, a similar agreement between  
283 simulation and experiments as for  $C_2H_4$  was found for  $CH_2O$  with a  $CH_2O:C_2H_4(\text{consumed})$  mole  
284 fraction ratio of 1:1. To be sure about the mentioned bias in the experiments of Rouso et al.  
285 [39], additional experiments and simulations have been done using a similar injection  
286 configuration. Similar profiles for  $C_2H_4$  and  $CH_2O$  as those of Rouso et al. [39] have been found  
287 (see FIGURE S7).

288 As is shown in FIGURE 6, a similar agreement between simulations and experiments as  
289 for  $C_2H_4$  can be observed for the mole fraction profile of the main products,  $CH_2O$ ,  $CO$ , and  
290  $CO_2$ . At the lowest temperatures,  $CH_2O$  is the main product formed by the ozonolysis of  $C_2H_4$ .  
291 At 350 K and in the case of 1000 ppm of  $O_3$ , the mole fraction of  $CH_2O$  is about 800 ppm, which  
292 is twice the mole fraction of  $CO$  and  $CO_2$ . At 800 K, the mole fractions of  $CO$  and  $CH_2O$  are  
293 equivalent (around 1000 ppm).  $CH_2O$ ,  $CO$ , and  $CO_2$  are formed through the global reactions  
294 implemented in the kinetic model to describe ozonolysis (see FIGURE S8/equations 1 to 4).  
295 Those reactions allow to fairly well reproduce the mole fraction profiles of the main products.  
296 In the case of 2000 ppm of  $O_3$ , however,  $CH_2O$  is overestimated by up to ~50%, indicating  
297 needed refinements in the considered product formation pathways. Water is also one of the  
298 major expected products at low temperatures, but as for the  $O_3$ -free experiments, it could not  
299 be quantified in this work. The predicted mole fraction of water is ~250 ppm (see FIGURE S9).

300 Note that a 2-fold increase in the mole fraction of O<sub>3</sub> leads to an approximately 2-fold increase  
301 in the mole fraction of major products at low temperatures.

302



303  
304 FIGURE 6. Comparison of experimental and predicted mole fractions as a function of  
305 temperature of low-temperature products measured during the O<sub>3</sub>-assisted oxidation of  
306 C<sub>2</sub>H<sub>4</sub>. The symbols correspond to the experimental results and the lines to the predictions of  
307 the kinetic model.

308  
309 Two minor products were also detected, acetaldehyde (see FIGURE 6) and oxirane (see  
310 FIGURE S10). Concerning CH<sub>3</sub>CHO, discrepancies between experiments and simulations can  
311 be observed with overestimation up to a factor of two above 600 K. For 2000 ppm of O<sub>3</sub>, the  
312 experimental data show a stable formation of CH<sub>3</sub>CHO up to 800 K while the simulated mole  
313 fraction profile starts increasing from 600 K. The flow rate analysis at 650 K (see FIGURE 5)  
314 shows that the discrepancies at high temperature are still linked to the overestimation of the

315 reaction  $C_2H_4 + OH$ . The main fate of the  $CH_2CH_2OH$  radical coming from the addition reaction  
316  $C_2H_4 + OH$  is an H-abstraction by  $O_2$  leading to ethenol ( $CH_2CHOH$ ). Note that according to the  
317 literature, ethenol has never been observed so far in GC and thus was not observed in this  
318 work either, probably due to a fast tautomerization into  $CH_3CHO$ . In the 1000 ppm  $O_3$  case,  
319 experiments display a local maximum mole fraction located at 400 K, which is not reproduced  
320 by the model.

321           Concerning oxirane, simulation also underestimates the mole fraction at the lowest  
322 temperatures. The simulated profile starts to increase only above 550 K, while the  
323 experimental data show a stable formation of about 12 ppm from 400 K and 500 K for both  
324 initial  $O_3$  concentrations. The mole fraction of oxirane is fairly well reproduced at higher  
325 temperatures.

326           The underestimation of the production of the two minor products at low temperature  
327 shows missing reaction pathways in the kinetic model. The reaction mechanisms should  
328 therefore be more detailed than the global ozonolysis reactions that are currently  
329 implemented in the kinetic model. The formation of oxirane observed at low temperatures  
330 can be explained by the 1,2,3-trioxy ozonide (POZ) biradical decomposition giving oxirane and  
331 singlet oxygen as proposed in the literature but the exit channel with the formation of oxygen  
332 atom is predicted to be minor due to a higher energy barrier. Alternatively, the reaction  
333 between Cl and  $C_2H_4$  can also be a source of oxirane with formaldehyde as co-product. The  
334 measurement of the oxirane mole fraction profile in this work will provide a constraint for  
335 future implementation of the kinetic parameters of the POZ biradical decomposition.  
336 Moreover, a potential missing source for acetaldehyde could be the dissociation of the  
337 hydroxymethyl formate ( $HOCH_2OHCO$ ), coming from the isomerization of the POZ, through a  
338 C-O bond rupture.

339           Methanol was also detected in smaller amounts than  $CH_2O$ , CO, and  $CO_2$  since 300 K  
340 in the 2000 ppm  $O_3$  case but with a higher mole fraction than  $CH_3CHO$  and oxirane (see FIGURE  
341 S10). In the 1000 ppm  $O_3$  case, methanol only starts at 550 K. Above this temperature, both  
342 profiles seem relatively similar. The mole fraction of methanol in both  $O_3$  cases oscillates  
343 between 30 and 70 ppm with a maximum around 700-750 K and is no longer detected above  
344 850 - 900 K. The shape of the simulated mole fraction profile is relatively similar to the  
345 experimental one at the highest temperatures, but with an order of magnitude lower and with  
346 a  $\sim 90$  K temperature shift. This temperature range fits with the formation of O-atoms (see

347 FIGURE S6). The flow rate analysis at 650 K (see FIGURE 5) shows that the main source of  
348 methanol is the reaction  $C_2H_4 + O$  leading to the formation of  $CH_3$  with HCO. The main fate of  
349  $CH_3$  is the addition of  $O_2$  to form  $CH_3OO$  and then methyl hydroperoxide ( $CH_3OOH$ ). The  
350 formation of hydroperoxides following the reaction  $C_2H_4 + O_3$  could not be addressed in this  
351 work due to their decomposition during the GC analysis but have been observed in the  
352 literature [39]. However, the formation of  $CH_3OH$  at low temperatures is not predicted by the  
353 kinetic model and the temperature range does not fit with the formation of O-atoms. The  
354 current formation of  $CH_3OH$  in the atmosphere is mainly due to the reactions of OH radical  
355 with  $CH_3$  and  $CH_3OO$  [51,52], which are currently implemented in the kinetic model. This result  
356 shows that a reaction pathway is missing and that, as for  $CH_3CHO$ ,  $CH_3OH$  would come from  
357 secondary reactions after the ozonolysis of  $C_2H_4$ .

358 Note that formic acid, HCOOH, has also been detected by GC-MS after condensation  
359 of the gas phase using a liquid nitrogen trap, but cannot be quantified since FID is not sensitive  
360 to formic acid. Its detection shows that it should be formed in notable amounts. As proposed  
361 by Neeb et al. [53], the production of HCOOH can occur via a bimolecular reaction between  
362 Cls and  $CH_2O$ , an important primary product at the lowest temperatures (see FIGURE 6).

363

## 364 CONCLUSION

365 The influence of the addition of  $O_3$  on the oxidation of  $C_2H_4$  was experimentally  
366 investigated in a JSR coupled with GC analysis at temperatures from 300 to 1000 K under  $O_3$   
367 addition of 1000 and 2000 ppm. The evolution with temperatures of the mole fraction of eight  
368 species was reported. The addition of  $O_3$  enhanced the production of formaldehyde ( $CH_2O$ ),  
369 methanol ( $CH_3OH$ ), acetaldehyde ( $CH_3CHO$ ), oxirane ( $C_2H_4O$ ), formic acid (HCOOH), CO, and  
370  $CO_2$ . This work also demonstrates that the initial ozonolysis reaction shifts the temperature  
371 window of the conversion of  $C_2H_4$  and product formation to a lower temperature regime, in  
372 which the traditional  $C_2H_4$  oxidation cannot be initiated. However, the major role of the  $O_3$   
373 addition in the oxidation of  $C_2H_4$  remains limited since the additional conversion of  $C_2H_4$  is  
374 below 10% with the initial mole fraction of  $O_3$  used in this work and it does not change the  
375 chemistry of the high temperature regime. Nonetheless  $CH_2O$ , which is an important  
376 atmospheric pollutant, is the main product of the low-temperature ozonolysis reaction with a  
377 significant mole fraction  $\sim 1000$  ppm. This quantitative result is important to consider  
378 especially for closed environments such as warehouses or fruit stores, where non-negligible

379 amounts of C<sub>2</sub>H<sub>4</sub> can be present [54]. If these places use air purifiers, a phenomenon that is  
380 growing lately because of COVID-19, then a significant amount of formaldehyde can be  
381 expected, as many indoor appliances have been shown to generate significant amounts of O<sub>3</sub>  
382 [55]. More generally, the quantification of oxidation products and stable intermediates under  
383 conditions relevant to atmospheric and combustion studies provides a database of  
384 temperature-dependent products that can be used as a valuable guidance for future  
385 validation and improvement of detailed chemical kinetic models.

386         It has been shown that the configuration of the experimental setup and especially the  
387 mixing gas lines is important if one wants accurate quantitative ozonolysis experiments and  
388 avoid any thermal degradation of O<sub>3</sub> before reacting with the fuel. The experimental data  
389 were confronted to a kinetic model with an implemented ozone/ozonolysis submechanism  
390 based on IUPAC recommendations. Overall, contrary to what was mentioned in the literature,  
391 a kinetic model based on global reactions of the ethylene ozonolysis accurately reproduces  
392 the conversion of C<sub>2</sub>H<sub>4</sub>, O<sub>3</sub>, and main products over a wide temperature range from 300 K to  
393 1000 K. The kinetic model is able to capture the trend of the mole fraction profile of the small  
394 products above 800K, but below this temperature, disagreements between experiments and  
395 simulations are noted. The disagreements are also slightly worse at 2000 ppm than at 1000  
396 ppm of O<sub>3</sub>. This demonstrates that the implementation of a higher level of detail is needed in  
397 the kinetic model with further intermediate pathways to predict the entire product  
398 distribution derived from the C<sub>2</sub>H<sub>4</sub> ozonolysis chemistry. However, this is beyond the scope of  
399 the current study because this would require a total remodeling of the current kinetic model  
400 which is based on a global approach of the ozonolysis process. For this, it would be necessary  
401 to have information on the kinetics and products of all the main and secondary reactions of  
402 the CI network. For example, the formation of methanol is difficult to intuit because the  
403 structure is different from the initial reactant. Due to its formation at low temperature, it is  
404 likely to be formed from dissociation reactions following the formation of Cl. Rousso et al. [39]  
405 also detected methanol and mentioned that its formation is difficult to address because it  
406 could come from several pathways. The improvement of the knowledge of the C<sub>2</sub>H<sub>4</sub> ozonolysis  
407 reaction network would benefit first from a fine identification of the elusive intermediates,  
408 which could not be detected in this work, to provide hints on the missing reaction pathways  
409 using for instance advanced spectroscopic techniques, such as PEPICO coupled with tunable  
410 photoionization sources.

411

412 **ACKNOWLEDGMENTS**

413 No acknowledgements.

414

415 **REFERENCES**

416 [1] R. Criegee, G. Wenner, Die Ozonisierung des 9,10-Oktalins, *Justus Liebigs Annalen*  
417 *Der Chemie*. 564 (1949) 9–15. <https://doi.org/10.1002/jlac.19495640103>.

418 [2] R. Huisgen, Kinetics and Mechanism of 1,3-Dipolar Cycloadditions, *Angewandte*  
419 *Chemie International Edition in English*. 2 (1963) 633–645.  
420 <https://doi.org/10.1002/anie.196306331>.

421 [3] L. Vereecken, A. Novelli, D. Taraborrelli, Unimolecular decay strongly limits the  
422 atmospheric impact of Criegee intermediates, *Phys. Chem. Chem. Phys.* 19 (2017) 31599–  
423 31612. <https://doi.org/10.1039/C7CP05541B>.

424 [4] R. L. Caravan, M.A. H. Khan, B. Rotavera, E. Papajak, I. O. Antonov, M.-W. Chen,  
425 K. Au, W. Chao, D. L. Osborn, J. Jr-Min Lin, C. J. Percival, D. E. Shallcross, C. A. Taatjes,  
426 Products of Criegee intermediate reactions with NO<sub>2</sub>: experimental measurements and  
427 tropospheric implications, *Faraday Discussions*. 200 (2017) 313–330.  
428 <https://doi.org/10.1039/C7FD00007C>.

429 [5] M. Ehn, J.A. Thornton, E. Kleist, M. Sipilä, H. Junninen, I. Pullinen, M. Springer, F.  
430 Rubach, R. Tillmann, B. Lee, F. Lopez-Hilfiker, S. Andres, I.-H. Acir, M. Rissanen, T.  
431 Jokinen, S. Schobesberger, J. Kangasluoma, J. Kontkanen, T. Nieminen, T. Kurtén, L.B.  
432 Nielsen, S. Jørgensen, H.G. Kjaergaard, M. Canagaratna, M.D. Maso, T. Berndt, T. Petäjä, A.  
433 Wahner, V.-M. Kerminen, M. Kulmala, D.R. Worsnop, J. Wildt, T.F. Mentel, A large source  
434 of low-volatility secondary organic aerosol, *Nature*. 506 (2014) 476–479.  
435 <https://doi.org/10.1038/nature13032>.

436 [6] B. Yang, P. Ma, J. Shu, P. Zhang, J. Huang, H. Zhang, Formation mechanism of  
437 secondary organic aerosol from ozonolysis of gasoline vehicle exhaust, *Environmental*  
438 *Pollution*. 234 (2018) 960–968. <https://doi.org/10.1016/j.envpol.2017.12.048>.

439 [7] Y. Ju, J.K. Lefkowitz, C.B. Reuter, S.H. Won, X. Yang, S. Yang, W. Sun, Z. Jiang, Q.  
440 Chen, Plasma Assisted Low Temperature Combustion, *Plasma Chem Plasma Process*. 36  
441 (2016) 85–105. <https://doi.org/10.1007/s11090-015-9657-2>.

442 [8] Y. Ju, W. Sun, Plasma assisted combustion: Dynamics and chemistry, *Progress in*  
443 *Energy and Combustion Science*. 48 (2015) 21–83.  
444 <https://doi.org/10.1016/j.pecs.2014.12.002>.

445 [9] S. Wenting, J. Yiguang, Nonequilibrium Plasma-Assisted Combustion: A Review of  
446 Recent Progress, (2013) 12.

447 [10] S. Starikovskaia, D.A. Lacoste, G. Colonna, Non-equilibrium plasma for ignition and  
448 combustion enhancement, *Eur. Phys. J. D*. 75 (2021) 231.  
449 <https://doi.org/10.1140/epjd/s10053-021-00240-2>.

450 [11] A. Starikovskiy, N. Aleksandrov, Plasma-assisted ignition and combustion, *Progress*  
451 *in Energy and Combustion Science*. 39 (2013) 61–110.  
452 <https://doi.org/10.1016/j.pecs.2012.05.003>.

453 [12] W. Sun, X. Gao, B. Wu, T. Ombrello, The effect of ozone addition on combustion:  
454 Kinetics and dynamics, *Progress in Energy and Combustion Science*. 73 (2019) 1–25.  
455 <https://doi.org/10.1016/j.pecs.2019.02.002>.

456 [13] X. Gao, Y. Zhang, S. Adusumilli, J. Seitzman, W. Sun, T. Ombrello, C. Carter, The  
457 effect of ozone addition on laminar flame speed, *Combustion and Flame*. 162 (2015) 3914–  
458 3924. <https://doi.org/10.1016/j.combustflame.2015.07.028>.

- 459 [14] X. Gao, J. Zhai, W. Sun, T. Ombrello, C.D. Carter, The Effect of Ozone Addition on  
460 Autoignition and Flame Stabilization, in: 54th AIAA Aerospace Sciences Meeting, American  
461 Institute of Aeronautics and Astronautics, San Diego, California, USA, 2016.  
462 <https://doi.org/10.2514/6.2016-0960>.
- 463 [15] X. Gao, B. Wu, W. Sun, T. Ombrello, C. Carter, Ozonolysis activated autoignition in  
464 non-premixed coflow, *J. Phys. D: Appl. Phys.* 52 (2019) 105201.  
465 <https://doi.org/10.1088/1361-6463/aaf785>.
- 466 [16] A. Alfazazi, A. Al-Omier, A. Secco, H. Selim, Y. Ju, S.M. Sarathy, Cool diffusion  
467 flames of butane isomers activated by ozone in the counterflow, *Combustion and Flame*. 191  
468 (2018) 175–186. <https://doi.org/10.1016/j.combustflame.2017.12.034>.
- 469 [17] T. Ombrello, S.H. Won, Y. Ju, S. Williams, Flame propagation enhancement by  
470 plasma excitation of oxygen. Part I: Effects of O<sub>3</sub>, *Combustion and Flame*. 157 (2010) 1906–  
471 1915. <https://doi.org/10.1016/j.combustflame.2010.02.005>.
- 472 [18] J.-B. Masurier, F. Foucher, G. Dayma, P. Dagaut, Investigation of iso-octane  
473 combustion in a homogeneous charge compression ignition engine seeded by ozone, nitric  
474 oxide and nitrogen dioxide, *Proceedings of the Combustion Institute*. 35 (2015) 3125–3132.  
475 <https://doi.org/10.1016/j.proci.2014.05.060>.
- 476 [19] S. Sayssouk, D. Nelson-Gruel, C. Caillol, P. Higelin, Y. Chamaillard, Towards control  
477 of HCCI combustion by ozone addition: a mathematical approach to estimate combustion  
478 parameters, *IFAC-PapersOnLine*. 49 (2016) 361–368.  
479 <https://doi.org/10.1016/j.ifacol.2016.08.054>.
- 480 [20] S. Ji, X. Lan, J. Lian, H. Xu, Y. Wang, Y. Cheng, Y. Liu, Influence of Ozone on  
481 Ignition and Combustion Performance of a Lean Methane/Air Mixture, *Energy Fuels*. 31  
482 (2017) 14191–14200. <https://doi.org/10.1021/acs.energyfuels.7b02389>.
- 483 [21] D. Singleton, C. Carter, S.J. Pendleton, C. Brophy, J. Sinibaldi, J.W. Luginsland, M.  
484 Brown, E. Stockman, M.A. Gundersen, The effect of humidity on hydroxyl and ozone  
485 production by nanosecond discharges, *Combustion and Flame*. 167 (2016) 164–171.  
486 <https://doi.org/10.1016/j.combustflame.2016.02.016>.
- 487 [22] J.-B. Masurier, F. Foucher, G. Dayma, P. Dagaut, Homogeneous Charge Compression  
488 Ignition Combustion of Primary Reference Fuels Influenced by Ozone Addition, *Energy  
489 Fuels*. 27 (2013) 5495–5505. <https://doi.org/10.1021/ef401009x>.
- 490 [23] C.B. Reuter, T.M. Ombrello, Flame enhancement of ethylene/methane mixtures by  
491 ozone addition, *Proceedings of the Combustion Institute*. 38 (2021) 2397–2407.  
492 <https://doi.org/10.1016/j.proci.2020.06.122>.
- 493 [24] C.W. Gillies, J.Z. Gillies, R.D. Suenram, F.J. Lovas, E. Kraka, D. Cremer, Van der  
494 Waals complexes in 1,3-dipolar cycloaddition reactions: ozone-ethylene, ACS Publications.  
495 (2002). <https://doi.org/10.1021/ja00007a010>.
- 496 [25] J.Z. Gillies, C.W. Gillies, R.D. Suenram, F.J. Lovas, W. Stahl, The microwave  
497 spectrum and molecular structure of the ethylene-ozone van der Waals complex, ACS  
498 Publications. (2002). <https://doi.org/10.1021/ja00190a056>.
- 499 [26] L. Nord, Ozone complexes in solid nitrogen, *Journal of Molecular Structure*. 96  
500 (1983) 37–44. [https://doi.org/10.1016/0022-2860\(82\)90055-2](https://doi.org/10.1016/0022-2860(82)90055-2).
- 501 [27] P.S. Bailey, J.A. Thompson, B.A. Shoulders, Structure of the Initial Ozone-Olefin  
502 Adduct, *J. Am. Chem. Soc.* 88 (1966) 4098–4099. <https://doi.org/10.1021/ja00969a042>.
- 503 [28] L.A. Hull, I.C. Hisatsune, J. Heicklen, Low-temperature infrared studies of simple  
504 alkene-ozone reactions, *J. Am. Chem. Soc.* 94 (1972) 4856–4864.  
505 <https://doi.org/10.1021/ja00769a010>.
- 506 [29] C.K. Kohlmiller, L. Andrews, Infrared spectrum of the primary ozonide of ethylene in  
507 solid xenon, *J. Am. Chem. Soc.* 103 (1981) 2578–2583. <https://doi.org/10.1021/ja00400a016>.
- 508 [30] H. Kuehne, H.H. Guenthard, Spectroscopic study of the ozone-ethylene reaction.

509 Matrix-infrared spectra of three isotopic ethylene ozonides, *J. Phys. Chem.* 80 (1976) 1238–  
510 1247. <https://doi.org/10.1021/j100552a025>.

511 [31] M. Hawkins, C.K. Kohlmeier, L. Andrews, Matrix infrared spectra and photolysis and  
512 pyrolysis of isotopic secondary ozonides of ethylene, *J. Phys. Chem.* 86 (1982) 3154–3166.  
513 <https://doi.org/10.1021/j100213a019>.

514 [32] H.E. O’Neal, C. Blumstein, A new mechanism for gas phase ozone–olefin reactions,  
515 *International Journal of Chemical Kinetics.* 5 (1973) 397–413.  
516 <https://doi.org/10.1002/kin.550050310>.

517 [33] L.B. Harding, W.A. Goddard, Mechanisms of gas-phase and liquid-phase ozonolysis,  
518 *J. Am. Chem. Soc.* 100 (1978) 7180–7188. <https://doi.org/10.1021/ja00491a010>.

519 [34] D.L. Osborn, C.A. Taatjes, The physical chemistry of Criegee intermediates in the gas  
520 phase, *International Reviews in Physical Chemistry.* 34 (2015) 309–360.  
521 <https://doi.org/10.1080/0144235X.2015.1055676>.

522 [35] C.A. Taatjes, Criegee Intermediates: What Direct Production and Detection Can Teach  
523 Us About Reactions of Carbonyl Oxides, *Annual Review of Physical Chemistry.* 68 (2017)  
524 183–207. <https://doi.org/10.1146/annurev-physchem-052516-050739>.

525 [36] C.C. Womack, M.-A. Martin-Drumel, G.G. Brown, R.W. Field, M.C. McCarthy,  
526 Observation of the simplest Criegee intermediate CH<sub>2</sub>OO in the gas-phase ozonolysis of  
527 ethylene, *Sci. Adv.* 1 (2015) e1400105. <https://doi.org/10.1126/sciadv.1400105>.

528 [37] T.L. Nguyen, H. Lee, D.A. Matthews, M.C. McCarthy, J.F. Stanton, Stabilization of  
529 the Simplest Criegee Intermediate from the Reaction between Ozone and Ethylene: A High-  
530 Level Quantum Chemical and Kinetic Analysis of Ozonolysis, *J. Phys. Chem. A.* 119 (2015)  
531 5524–5533. <https://doi.org/10.1021/acs.jpca.5b02088>.

532 [38] M. Pfeifle, Y.-T. Ma, A.W. Jasper, L.B. Harding, W.L. Hase, S.J. Klippenstein,  
533 Nascent energy distribution of the Criegee intermediate CH<sub>2</sub>OO from direct dynamics  
534 calculations of primary ozonide dissociation, *J. Chem. Phys.* 148 (2018) 174306.  
535 <https://doi.org/10.1063/1.5028117>.

536 [39] A.C. Rousso, N. Hansen, A.W. Jasper, Y. Ju, Low-Temperature Oxidation of Ethylene  
537 by Ozone in a Jet-Stirred Reactor, *J. Phys. Chem. A.* 122 (2018) 8674–8685.  
538 <https://doi.org/10.1021/acs.jpca.8b06556>.

539 [40] A. C. Rousso, N. Hansen, A. W. Jasper, Y. Ju, Identification of the Criegee  
540 intermediate reaction network in ethylene ozonolysis: impact on energy conversion strategies  
541 and atmospheric chemistry, *Physical Chemistry Chemical Physics.* 21 (2019) 7341–7357.  
542 <https://doi.org/10.1039/C9CP00473D>.

543 [41] N. Genossar, J. P. Porterfield, J. H. Baraban, Decomposition of the simplest  
544 ketohydroperoxide in the ozonolysis of ethylene, *Physical Chemistry Chemical Physics.* 22  
545 (2020) 16949–16955. <https://doi.org/10.1039/D0CP02798G>.

546 [42] X. Shen, X. Yang, J. Santner, J. Sun, Y. Ju, Experimental and kinetic studies of  
547 acetylene flames at elevated pressures, *Proceedings of the Combustion Institute.* 35 (2015)  
548 721–728. <https://doi.org/10.1016/j.proci.2014.05.106>.

549 [43] H. Zhao, J. Fu, F.M. Haas, Y. Ju, Effect of prompt dissociation of formyl radical on  
550 1,3,5-trioxane and CH<sub>2</sub>O laminar flame speeds with CO<sub>2</sub> dilution at elevated pressure,  
551 *Combustion and Flame.* 183 (2017) 253–260.  
552 <https://doi.org/10.1016/j.combustflame.2017.05.005>.

553 [44] H. Zhao, X. Yang, Y. Ju, Kinetic studies of ozone assisted low temperature oxidation  
554 of dimethyl ether in a flow reactor using molecular-beam mass spectrometry, *Combustion and  
555 Flame.* 173 (2016) 187–194. <https://doi.org/10.1016/j.combustflame.2016.08.008>.

556 [45] C.B. Reuter, T.M. Ombrello, S.G. Tuttle, Can ozonolysis reactions influence  
557 detonations?, *Shock Waves.* 32 (2022) 363–371. <https://doi.org/10.1007/s00193-022-01082-6>.

558 [46] J. Bourgalais, O. Herbinet, H.-H. Carstensen, J. Debleza, G.A. Garcia, P. Arnoux, L.S.

559 Tran, G. Vanhove, B. Liu, Z. Wang, M. Hochlaf, L. Nahon, F. Battin-Leclerc, Jet-Stirred  
560 Reactor Study of Low-Temperature Neopentane Oxidation: A Combined Theoretical,  
561 Chromatographic, Mass Spectrometric, and PEPICO Analysis, *Energy Fuels*. 35 (2021)  
562 19689–19704. <https://doi.org/10.1021/acs.energyfuels.1c02080>.  
563 [47] R.J. Kee, F.M. Rupley, J.A. Miller, M.E. Coltrin, J.F. Grcar, E. Meeks, H.K. Moffat,  
564 A.E. Lutz, G. Dixon-Lewis, M.D. Smooke, CHEMKIN Collection, release 3.6; Reaction  
565 Design. Inc.; San Diego, CA, (2000).  
566 [48] O. Herbinet, G. Dayma, Jet-Stirred Reactors, in: F. Battin-Leclerc, J.M. Simmie, E.  
567 Blurock (Eds.), *Cleaner Combustion*, Springer London, London, 2013: pp. 183–210.  
568 [https://doi.org/10.1007/978-1-4471-5307-8\\_8](https://doi.org/10.1007/978-1-4471-5307-8_8).  
569 [49] J.P. Senosiain, S.J. Klippenstein, J.A. Miller, Reaction of Ethylene with Hydroxyl  
570 Radicals: A Theoretical Study, *J. Phys. Chem. A*. 110 (2006) 6960–6970.  
571 <https://doi.org/10.1021/jp0566820>.  
572 [50] J. Jian, H. Hashemi, H. Wu, A.W. Jasper, P. Glarborg, A reaction mechanism for  
573 ozone dissociation and reaction with hydrogen at elevated temperature, *Fuel*. 322 (2022)  
574 124138. <https://doi.org/10.1016/j.fuel.2022.124138>.  
575 [51] R.L. Caravan, M.A.H. Khan, J. Zádor, L. Sheps, I.O. Antonov, B. Rotavera, K.  
576 Ramasesha, K. Au, M.-W. Chen, D. Rösch, D.L. Osborn, C. Fittschen, C. Schoemaeker, M.  
577 Duncianu, A. Grira, S. Dusanter, A. Tomas, C.J. Percival, D.E. Shallcross, C.A. Taatjes, The  
578 reaction of hydroxyl and methylperoxy radicals is not a major source of atmospheric  
579 methanol, *Nat Commun*. 9 (2018) 4343. <https://doi.org/10.1038/s41467-018-06716-x>.  
580 [52] J.-F. Müller, Z. Liu, V.S. Nguyen, T. Stavrou, J.N. Harvey, J. Peeters, The reaction  
581 of methyl peroxy and hydroxyl radicals as a major source of atmospheric methanol, *Nat*  
582 *Commun*. 7 (2016) 13213. <https://doi.org/10.1038/ncomms13213>.  
583 [53] P. Neeb, O. Horie, G.K. Moortgat, The Ethene–Ozone Reaction in the Gas Phase, *J.*  
584 *Phys. Chem. A*. 102 (1998) 6778–6785. <https://doi.org/10.1021/jp981264z>.  
585 [54] C.G. Rao, *Engineering for Storage of Fruits and Vegetables: Cold Storage, Controlled*  
586 *Atmosphere Storage, Modified Atmosphere Storage*, Academic Press, 2015.  
587 [55] H. Salonen, T. Salthammer, L. Morawska, Human exposure to ozone in school and  
588 office indoor environments, *Environment International*. 119 (2018) 503–514.  
589 <https://doi.org/10.1016/j.envint.2018.07.012>.  
590